Advanced endoscopic imaging of esophageal neoplasia; old looks and new visions

Boerwinkel, D.F.

Publication date
2014

10

OPTIMIZED ENDOSCOPIC AUTOFLUORESCENCE SPECTROSCOPY FOR THE IDENTIFICATION OF PREMALIGNANT LESIONS IN BARRETT'S OESOPHAGUS

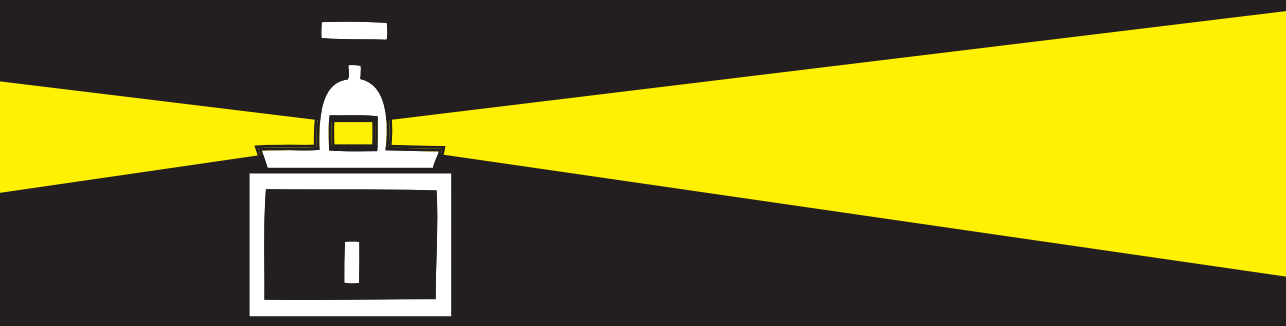

Jasmin A Holz; David F Boerwinkel; Sybren L. Meijer; Mike Visser; Ton G van Leeuwen; Maurice CG Aalders; Jacques JGHM Bergman

Published in:
European Journal of Gastroenterology and Hepatology, 2013 Dec.

ABSTRACT

OBJECTIVE: Fluorescence spectroscopy has the potential to detect early cellular changes in Barrett's oesophagus before these become visible. As the technique is based on varying concentrations of intrinsic fluorophores, each with its own optimal excitation wavelength, it is important to assess the optimal excitation wavelength(s) for identification of premalignant lesions in patients with Barrett's oesophagus.

METHODS: The endoscopic spectroscopy system used contained five (ultra)violet light sources (λ_{exc} = 369 nm to 416 nm) to generate autofluorescence during routine endoscopic surveillance. Autofluorescence spectroscopy was followed by a biopsy for histological assessment and spectra correlation. Three intensity ratios (r1, r2, r3) were calculated by dividing the area, *A*, under the spectral curve of selected emission wavelength ranges for each spectrum generated by each excitation wavelength λ_{exc} as follows $r1_{\lambda exc} = (A_{560\pm5}/A_{640\pm5})$, $r2_{\lambda exc} = (A_{495\pm5}/A_{560\pm5})$ and $r3_{\lambda exc} = (A_{495\pm5}/A_{640\pm5})$. Double intensity ratios were calculated using two excitation wavelengths.

RESULTS: Fifty-eight tissue areas from 22 patients were used for autofluorescence spectra analysis. Excitation with 395, 405 or 410 nm showed a significant ($P \leq 0.0006$) differentiation between intestinal metaplasia and grouped high-grade dysplasia/early carcinoma for intensity ratios r2 and r3. A sensitivity of 80.0 % and specificity of 89.5 % with an area under the ROC curve of 0.85 was achieved using 395 nm excitation and intensity ratio r3.

CONCLUSION: Double excitation showed no additional value over single excitation. The combination of 395 nm excitation and intensity ratio r3 showed optimal conditions to discriminate non-dysplastic from early neoplasia in Barrett's oesophagus.

INTRODUCTION

Barrett's oesophagus (BO) is known as a condition which may lead to oesophageal adenocarcinoma. The long-term survival rate of patients with adenocarcinoma is poor because of late diagnosis. In BO, the normal squamous lining of the oesophagus is replaced by intestinal metaplasia (IM), which can develop into adenocarcinoma through a series of premalignant stages of dysplasia: IM develops into low-grade dysplasia (LGD), then high-grade dysplasia (HGD) and eventually into early carcinoma (EC). HGD and early carcinoma are accessible for endoscopic treatment, with a significant lower morbidity and mortality than late stage surgical therapy [1-4]. Patients with BO are recommended to undergo regular surveillance endoscopy in order to detect these premalignant lesions at an early and curable stage. However, these premalignant stages of dysplasia are hard to detect with standard white light endoscopy and are often overlooked during surveillance endoscopy. The current best practice for tissue evaluation and diagnosis is meticulous white light inspection of the oesophagus to detect visible abnormalities. In the absence of visible lesions, random biopsies in four quadrants, every 2 cm, are undertaken. However, random biopsies are laborious, burdensome, expensive and may easily miss early and focal dysplasia, as they sample only ~5 % of the BO [5]. Moreover, the histopathological interpretation of dysplasia has a high interobserver and intraobserver variability [6]. There is therefore, an urgent need for a minimally invasive and objective technique that allows diagnosis in real time.

Endoscopic diagnostic procedures such as white light endoscopy have a sensitivity and specificity of around 50-80 % [7-11]. Recent developments in identifying lesions in BO during endoscopy focuses on imaging techniques such as high-definition white light endoscopy, endomicroscopy, autofluorescence imaging, and narrow band imaging. These imaging techniques are not yet clinically accepted because of their additional examination time, complexity, costs or inefficiency. The low sensitivity and specificity in identifying early lesions is mainly caused by low contrast between BO tissue and premalignant lesions [7-11]. In the case of autofluorescence imaging, this contrast might be improved with knowledge of the optimal excitation and emission wavelengths which can then replace the currently used broad-band illumination and detection.

Fluorescence spectroscopy has the potential to detect early cellular changes in BO before these become visible. Fluorophores, naturally present in varying concentrations in tissue, generate a fluorescence spectrum upon excitation with blue or UV light. The shape and intensity of these so-called autofluorescence spectra depend on the excitation wavelength, tissue type and level of differentiation towards cancer [12-14]. Over the last few decades, autofluorescence has shown its potential to detect early changes in premalignant lesions of several epithelial tissue types such as the colon [15-21], oral cavity [22-26], cervix [27-30], and bronchus [31-34]. In the gastrointestinal (GI) tract, point spectroscopy was extensively used on colon tissue and later expanded into the oesophagus [35-43]. *Panjehpour et al*. used in-vivo fluorescence spectroscopy and reported that 410 nm excitation could differentiate non-dysplastic from HGD in BO with 100 % sensitivity and 96 % specificity [38]. Although the high sensitivity and specificity were promising, they could not be repeated in follow up studies. The studies vary in methods and materials as well in examined tissue types and show a wide range in determined

sensitivity (75 %-100 %) and specificity (65 %-95 %) [44]. Previous research on oesophageal autofluorescence in 37 patients has shown in the diagnosis of HGD in BO that 400 nm excitation (sensitivity = 74 %, specificity = 85 %) is more effective than 337 nm (sensitivity = 74 %, specificity = 67 %) [37]. *Wang et al*. showed that the specificity of oral cancer diagnosis can be increased using multiple excitation wavelengths and double excitation algorithms [22]. *Bogaards et al*. showed that using 405 nm and 435 nm excitation and double ratio of fluorescence images, non-invasive staging of cervical intraepithelial neoplasia is feasible [45].

Considering the low absolute risk of developing HGD/EC, detecting the rare abnormalities is crucial to any imaging modality that may aid endoscopic surveillance of BO, which implies a high sensitivity. Furthermore, high specificity may influence the number of biopsies taken from healthy tissue, potentially reducing the drawbacks associated with the current standard biopsy protocol. On the basis of the above mentioned results, albeit on other organs, we hypothesize that an optimized excitation around 400 nm can improve the differentiation between non-dysplastic BO and premalignant tissue. Furthermore, we hypothesise that the combination of spectra obtained by different excitation wavelengths can further improve this differentiation. To test these hypotheses we aim to identify characteristics in autofluorescence spectra of BO to determine which (combination of) excitation wavelength(s) around 400 nm is optimal for the identification of premalignant lesions in BO.

METHODS

Patients

Twenty-three patients scheduled for routine BO endoscopy at the Department of Gastroenterology and Hepatology at the Academic Medical Centre (AMC) Amsterdam were included. The patients were 74 % men with a mean age of 67 years (SD: ± 11 years) and a median Barrett's segment of C3M4 (interquartile range: C1-5, M2.5-8.5). All patients were on proton pump inhibitor therapy. The criterion for patient inclusion in the study was a prior diagnosed BO with and without known early neoplasia. Patients who had a prior history of upper GI surgery or endoscopic treatment were excluded. The study was approved by the Medical Ethics Committee of the AMC Amsterdam. Written informed consent was obtained from all patients.

Spectroscopy system

Autofluorescence spectroscopy was performed using a multi-wavelength spectroscopy system (2M Engineering Ltd, Veldhoven, The Netherlands), which consisted of a UV-LED with a wavelength of 369 nm as well as laser diodes with wavelengths of 395, 405, 410 and 416 nm. A customized fibre probe (CeramOptec GmbH, Bonn, Germany) was designed to fit through the accessory channel of a standard endoscope, to deliver the excitation light to the tissue site and to transmit the emitted light to the attached spectrometer USB4000 (Ocean Optics Inc., Dunedin, Florida, USA). The fibre probe tip was 2 mm in diameter and consisted of 15 illumination and 15 collection fibres. The 15 collection fibres were aligned to the 200 µm entrance slit of the spectrometer to detect all collected light. LabView (National Instruments

Corporation, Austin, Texas, USA) was used to develop a program to switch the light sources and to collect the autofluorescence spectra sequentially.

Endoscopic and histological procedures

All procedures were performed by one endoscopist (J.J.G.H.M.B.) with extensive experience in the diagnosis and treatment of early Barrett's neoplasia. All patients were sedated by intravenous administration of propofol or midazolam (2.5-15 mg), supplemented with fentanyl (0.1-0.2 mg) if necessary. After cleaning with acetylcysteine, the oesophagus was first inspected with white light endoscopy and all suspicious areas for dysplasia were recorded. Suspicious and unsuspicious areas for dysplasia were selected for investigation with the spectroscopy system. Subsequently, the fibre probe was introduced through the accessory channel of the endoscope and placed in gentle contact with the tissue site under investigation. A transparent cap (Olympus Inc., Tokyo, Japan) attached to the distal end of the endoscope was used to minimize the movement of the fibre probe on tissue. Before measurement, the endoscope light was switched off. The light sources of the spectroscopy system were then switched on sequentially and the corresponding autofluorescence spectra were collected. Spectra acquisition took several seconds per spectrum and the whole procedure with several measurements per patient took around 10 min. Measurements were repeated when the patient moved or the probe was not stable on the tissue site. From each measured tissue site a biopsy was taken for histological assessment. The endoscope with the cap was stabilized at the spectroscopic measurement site by gentle suction, ensuring precise correlation between the measured tissue site and the corresponding biopsy location. Collected biopsies were fixed in formalin, embedded in paraffin and cut and stained with haematoxylin and eosin (H&E). Histological assessment was performed by expert GI pathologists and classified according to the Vienna classification [46].

Spectra analysis

Analysis for discriminating autofluorescence spectra of histological classified IM from grouped HGD/EC was performed per excitation wavelength (single) and in a combination of two excitation wavelengths (double).

Spectrometer noise was subtracted from each autofluorescence spectrum. Spectra with positive, unsaturated intensities between 480 and 650 nm emission and a signal-to-noise ratio at maximal intensity of at least five were included in the analysis. Selected spectra were normalized by dividing the intensities by the area under the spectral curve from 480 to 650 nm and then multiplying by 1000. Normalized spectra were smoothed with a moving average of 6 nm.

Normalized and smoothed autofluorescence spectra of IM and HGD/EC classified biopsies were averaged to create an Excitation-Emission-Matrix (EEM) using OriginPro8 (OriginLab Corporation, Northampton, Massachusetts, USA). The EEMs visualise the emission intensities related to the excitation wavelengths and tissue types. Three characteristic emission wavelengths, that is 495, 560 and 640 nm were selected for calculation of intensity ratios. Three intensity ratios (r1, r2 and r3) were calculated by dividing the area, *A*, under the curve of two selected emission wavelengths (±5 nm) for each spectrum generated by each excitation wavelength λ_{exc}, as follows

$r1_{\lambda exc} = (A_{560\pm5}/A_{640\pm5})$, $r2_{\lambda exc} = (A_{495\pm5}/A_{560\pm5})$ and $r3_{\lambda exc} = (A_{495\pm5}/A_{640\pm5})$. Double intensity ratios (dr1, dr2 and dr3) were calculated by dividing the intensity ratios of two excitation wavelengths obtained from the same tissue site. For example, double intensity ratio of $r1_{\lambda exc}$, called $dr1_{\lambda exc1/\lambda exc2} = r1_{\lambda exc1}/r1_{\lambda exc2}$, for the combination of 369 and 405 nm was defined as $dr1_{369/405} = r1_{369}/r1_{405}$.

The statistical relevance of the differences in intensity ratios of the two tissue types was determined using unpaired two-tailed Student's *t*-test. A *P*-value of less than 0.05 was considered statistically significant. Receiver operating characteristic (ROC) curves were used to compare the performance of the five excitation wavelengths and the three intensity ratios for single and double excitation. In addition, the area under the ROC curve (AUC) was used to describe the discrimination ability, where 1 is perfect. All statistical analysis was performed using Prism 5 (GraphPad Software Inc., La Jolla, California, USA).

RESULTS

In total, 23 patients were included in the study from which 83 locations within the Barrett's segment were investigated with the spectroscopy system followed by a corresponding biopsy (Table 1). For example, Table 1 shows that 38 biopsies from 15 patients were classified as IM. One patient who did not show any biopsy classified as IM, HGD, or EC was excluded from the analysis.

Single excitation

Table 2 shows the number of spectra, which fulfil the requirements for the analysis, included in the single excitation analysis. Typical normalized autofluorescence spectra showed an intensity peak around 495 nm emission, which decreased with increasing excitation wavelength for both tissue types (*figure 1*). After normalization the emission intensities for HGD/EC were reduced in the green and increased in the red wavelength range compared with IM.

The emission intensities changed most around 495 nm, comparing the EEM of IM and HGD/EC (*figure 2*). Furthermore, around 560 nm emission the intensities were independent of excitation wavelength and tissue type. At longer excitation wavelengths a small increase in red emission around 640 nm for HGD/EC was observed.

Table 1. Number of biopsies taken per histological diagnosis with the corresponding n number of patients.

Histological diagnosis	Number of biopsies (n=83)	Number of patients (n=23*)
Squamous/gastric	9	7
IM	38	15
Indefinite for dysplasia	2	2
LGD	14	7
HGD	14	9
EC	6	5

IM, intestinal metaplasia; LGD, low-grade dysplasia; HGD, high-grade dysplasia; EC, early carcinoma.
*Multiple biopsies were taken per patient.

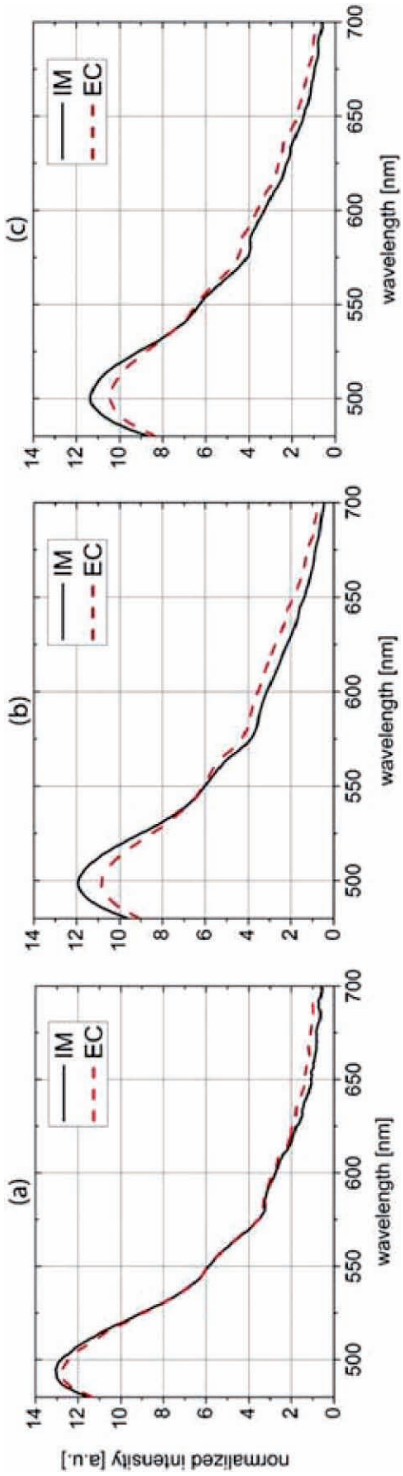

Figure 1. Typical normalized autofluorescence spectra obtained from one patient IM (–) and EC (--) at (a) 369 nm, (b) 405 nm and (c) 416 nm excitation. IM, intestinal metaplasia; EC, early carcinoma.

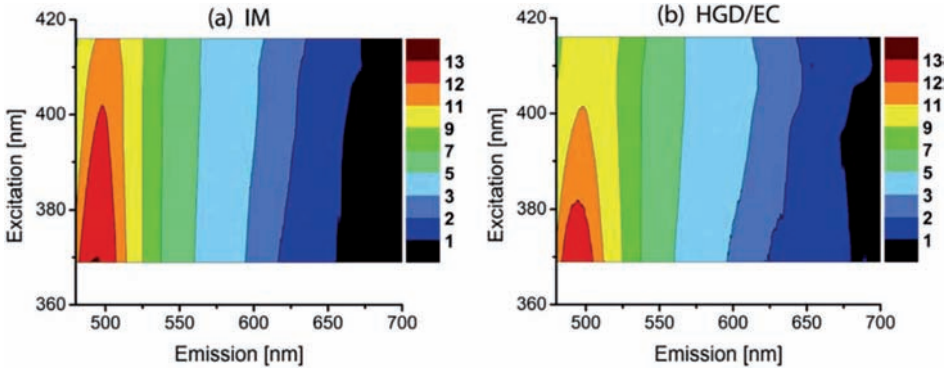

Figure 2. EEM of averaged normalized autofluorescence spectra at 369, 395, 405, 410 and 416 nm excitation for (a) IM and (b) HGD/EC. IM, intestinal metaplasia; HGD, high-grade dysplasia; EC, early carcinoma; EEM, Excitation-Emission-Matrix.

The three intensity ratios $r1_{\lambda exc} = (A_{560\pm5}/A_{640\pm5})$, $r2_{\lambda exc} = (A_{495\pm5}/A_{560\pm5})$ and $r3_{\lambda exc} = (A_{495\pm5}/A_{640\pm5})$ were calculated for all spectra of IM and HGD/EC (*figure 3*). Intensity ratios of r2 had the lowest values, whereas intensity ratios of r3 had the highest values. Compared to IM, HGD/EC showed significantly decreased intensity ratios ($P \leq 0.0006$) of r2 and r3 at 395, 405 and 410 nm excitation. The intensity ratios of IM showed higher standard errors of the mean than those of HGD/EC ratios (*figure 3*).

Figure 4 illustrates the sensitivity and specificity with ROC curves for single excitation and the three intensity ratios (r1, r2, r3) for distinguishing IM from HGD/EC. The largest AUCs (0.89, 0.88 and 0.89) were obtained with intensity ratio r2 after 395, 405 and 410 nm excitation, respectively. Using 410 nm and r2 with a threshold value of less than 2.11 and zero false negatives resulted in 100 % sensitivity and 58.8 % specificity in identifying HGD/EC versus IM. Setting the false positive cases to zero and the threshold value to less than 1.84 resulted in 100 % specificity and 38.9 % sensitivity using 410 nm excitation and r2.

The highest combination of sensitivity and specificity, 80.0 % and 89.5 % respectively, was determined using 395 nm excitation applying intensity ratio r3 ($A_{495\pm5}/A_{640\pm5}$) with a threshold value of less than 6.29 for identifying HGD/EC versus IM (Table 3). Four measurements out of 20 (20%) were false negative and four measurements out of 38 (11%) were false positive.

Within five patients, spectra of one or more areas of both IM and HGD/EC were recorded and averaged per tissue type. Excitation with 395 nm in combination with the intensity ratio r3 and the selected threshold value of less than 6.29, resulted in discrimination with 100 % sensitivity and specificity. These intrapatient analyses showed on average that intensity ratios of IM (7.9 ±1.0) were higher in value and in SD than ratios of HGD/EC (5.8 ±0.2).

Double excitation

Thirty-two IM spectra and 12 HGD/EC spectra were used for double excitation analysis. Double ratios at 10 combinations of excitation wavelengths (excitation at 369 and 395 nm, 369 and 405 nm, 369 and 410 nm, 369 and 416 nm, 395 and 405 nm, 395 and 410 nm, 395 and 416 nm,

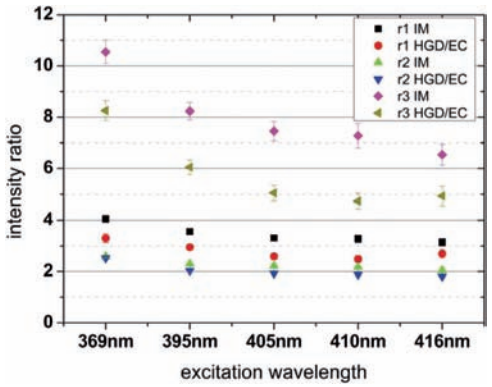

Figure 3. Averaged intensity ratios with SEM of r1 = (A560±5/A640±5), r2 = (A495±5/A560±5) and r3 = (A495±5/A640±5) at 369, 395, 405, 410 and 416 nm excitation for IM and HGD/EC. IM, intestinal metaplasia; HGD, high-grade dysplasia; EC, early carcinoma.

Table 2. Numbers of spectra included in the single excitation analysis.

λ_{exc} (nm)	Number of spectra IM	HGD and EC (HGD/EC)
369	35	19 (13/6)
395	38	20 (14/6)
405	37	20 (14/6)
410	34	18 (12/6)
416	33	12 (8/4)

$\lambda_{exc.}$, excitation wavelength; IM, intestinal metaplasia; HGD, high-grade dysplasia; EC, early carcinoma.

Table 3. Sensitivity, specificity and AUC of r3 = (A495±5/A640±5) for distinguishing IM from HGD/EC.

λexc (nm)	Sensitivity (%)	Specificity (%)	AUC	Threshold value
369	26.3	88.6	0.76	< 7.45
395	80.0	89.5	0.85	< 6.29
405	70.0	89.2	0.85	< 5.35
410	72.2	88.2	0.86	< 5.22
416	50.0	90.9	0.75	< 4.62

λexc., excitation wavelength; IM, intestinal metaplasia; HGD, high-grade dysplasia; EC, early carcinoma; AUC, area under the curve.

405 and 410 nm, 405 and 416 nm, and 410 and 416 nm) were calculated. All combinations with 369 nm excitation and double intensity ratio dr2 resulted in the highest AUCs (≥ 0.76; *figure 5*). A combination of 369 and 395 nm for excitation and intensity ratio dr2 resulted in an AUC of 0.80

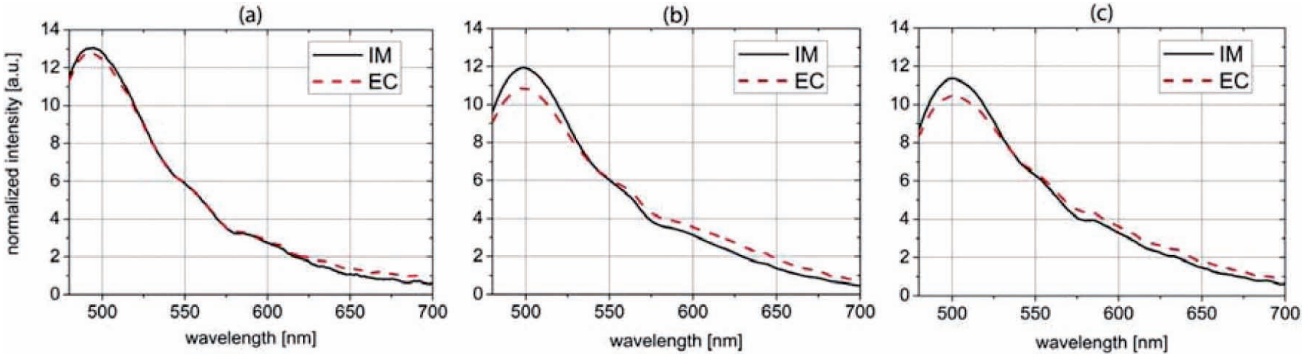

Figure 4. ROC curves for intensity ratios (a) r1 = (A560±5/A640±5), (b) r2 = (A495±5/A560±5) and (c) r3 = (A495±5/A640±5) at 369, 395, 405, 410 and 416 nm excitation for IM vs. HGD/EC. IM, intestinal metaplasia; HGD, high-grade dysplasia; EC, early carcinoma; ROC, receiver operating characteristic.

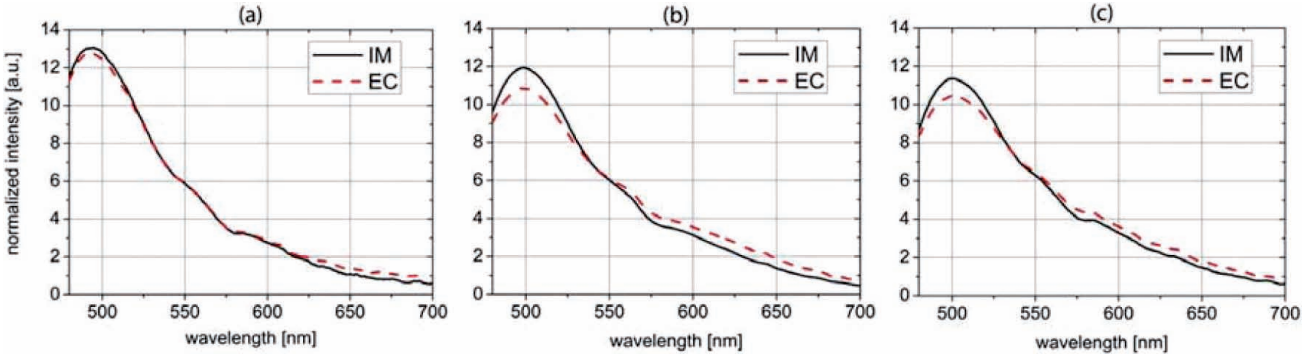

Figure 5. ROC curves for double intensity ratios (a) dr1, (b) dr2 and (c) dr3 of IM vs. HGD/EC for the excitation combinations 369 and 395 nm, 369 and 405 nm, 369 and 410 nm, 369 and 416 nm, and 395 and 405 nm. IM, intestinal metaplasia; HGD, high-grade dysplasia; EC, early carcinoma; ROC, receiver operating characteristic.

and in a sensitivity of 83 % and specificity of 75 %. Comparing ROC curves from single and double excitation, no increase in specificity was observed using double excitation. Furthermore, all 10 combinations of excitation wavelengths showed no significant difference in all three double intensity ratios for the discrimination of IM and HGD/EC.

DISCUSSION

In the present study we have shown that several excitation wavelengths around 400 nm can significantly distinguish premalignant lesions from IM in BO. First we evaluated whether changing the wavelength of the excitation light around 400 nm would improve the differentiation between non-dysplastic BO and early neoplasia, such as HGD and early carcinoma. To this end we studied the characteristics of autofluorescence spectra of BO and found that single excitation at 395, 405 or 410 nm demonstrated that IM could be significantly distinguished from HGD/EC, with a prominent decrease in intensity ratio r3 ($A_{495\pm5}/A_{640\pm5}$) in premalignant lesions. These findings agree with previous research, which reported that the decrease around 495 nm emission might be related to decreased collagen fluorescence [15;27;47]. This phenomenon may be because of a break down in collagen cross-links [15;30] or thickening of the epithelial layer. The latter reduces the penetration depth of the excitation light and therefore reduces the detected fluorescence from fluorophores present in deeper layers [48]. It is also known that porphyrins, which emit fluorescence around 630 nm, are excited efficiently around 405 nm. Porphyrins are found predominantly in (pre-)malignant tissue, rather than in non-dysplastic tissue, and might therefore be the cause of the increased red emission [24;49-52].

In contrast to our second hypothesis, the improvement of differentiation by combining two excitation wavelengths, the sensitivity and specificity in discrimination IM from HGD/EC could not be increased within the wavelength range we used (369 nm to 416 nm). *Wang et al*. used single and double excitation wavelengths for distinguishing cancerous from normal oral mucosa. Combining shorter (280, 290 and 300 nm) with longer (320, 330 and 340 nm) wavelengths, a higher specificity was achieved compared to single excitation [22]. An explanation for why we did not reach higher specificity with the double excitation approach might be that in our excitation wavelength range, the emission spectra did not show characteristically different peaks, and we measured on different types of tissue.

Although the sensitivity of 80.0 % and specificity of 89.5 % achieved is comparable or superior to standard white light endoscopic inspection, room for improvement still exists, for instance by taking into account interpatient differences in the morphological and optical properties of the oesophagus. The high variations of intensity ratios for IM might be caused by variations in tissue morphology which influence the penetration depth of the excitation light and therefore also the intensity of the detected fluorescence. In contrast, inflammations in the Barrett's segment might be a cause of increased red fluorescence. It is known that various bacteria, such as *Escherichia coli*, produce porphyrin that emits red fluorescence [24;52]. One way to circumvent these interpatient differences is to compare only spectral characteristics of healthy and suspicious tissue from data within that patient. A preliminary intrapatient analysis in five patients indeed discriminated HGD/EC from IM with 100 % sensitivity and specificity using

395 nm excitation and intensity ratio r3 = ($A_{495\pm5}/A_{640\pm5}$) with a threshold value of less than 6.29, but more data is needed to substantiate this finding.

In the current study, multi-wavelength excitation did not improve the sensitivity or specificity compared with single wavelength excitation. However, multi-wavelength excitation may provide information from several different depths in the tissue. A promising direction for future research is to combine excitation at a 'long' wavelength such as 395 nm with a shorter wavelength (e.g. 280 nm for tryptophan or 330 nm for collagen) and to use an internal reference measurement on healthy tissue (in the same patient). So far, laser diodes in the UV wavelength range are still under development and when available will make clinical applications of lasers more compact, easy and affordable. Furthermore, data analysis with multi-variant methods may also improve sensitivity and specificity in discriminating IM from HGD/EC in BO. A limitation of our current endoscopy procedure is the precise match of the spectroscopic measurement site with the location of the taken biopsy. This mismatch can be minimised by integrating the spectroscopy probe into the biopsy forceps.

Finally, for further improvement in the discrimination of HGD/EC from IM, more fundamental knowledge is needed about tissue layers, their biochemical and morphological changes, as well as quantitative fluorophore distribution, and scattering and absorption characteristics in normal versus (pre)malignant mucosa in the oesophagus. This information can be obtained by other imaging techniques. Optical coherence tomography (OCT), for instance, can precisely identify the layer thickness and morphology of the oesophageal wall [53;54]. OCT can also provide functional information based on changes in the scattering properties of tumour tissue [55;56], or the structure of blood vessels [57]. The combination of OCT with fluorescence or Raman spectroscopy [58] may then be a next step towards quantitative imaging.

CONCLUSION

Fluorescence spectroscopy with 395, 405 and 410 nm excitation allows discrimination between IM and HGD/EC in patients with BO. The highest combination of sensitivity and specificity, 80.0 % and 89.5 % respectively, was determined using 395 nm excitation applying intensity ratio r3 ($A_{495\pm5}/A_{640\pm5}$) with a threshold value of less than 6.29. In our study, double excitation demonstrated no additional value over single excitation.

ACKNOWLEDGEMENTS

This research was funded by the *7th Framework Programme for Research and Technological Development, of the* European Union, Grant Agreement Number 231993 (EDOCAL). The authors like to thank Dirk Faber for his contribution to the development of the software program in LabView and Martin van Gemert for his comments on the manuscript.

REFERENCES

1. Ell C, May A, Gossner L, Pech O, Gunter E, Mayer G, et al. Endoscopic mucosal resection of early cancer and high-grade dysplasia in Barrett's esophagus. Gastroenterology 2000;118:670-677.
2. Behrens A, Pech O, Graupe F, May A, Lorenz D, Ell C. Barrett's adenocarcinoma of the esophagus: better outcomes through new methods of diagnosis and treatment. Dtsch Arztebl Int 2011;108:313-319.
3. Ell C, May A, Pech O, Gossner L, Guenter E, Behrens A, et al. Curative endoscopic resection of early esophageal adenocarcinomas (Barrett's cancer). Gastrointest Endosc 2007;65:3-10.
4. Westerterp M, Koppert LB, Buskens CJ, Tilanus HW, ten Kate FJ, Bergman JJ, et al. Outcome of surgical treatment for early adenocarcinoma of the esophagus or gastro-esophageal junction. Virchows Arch 2005;446:497-504.
5. Tschanz ER. Do 40% of patients resected for barrett esophagus with high-grade dysplasia have unsuspected adenocarcinoma? Arch Pathol Lab Med 2005;129:177-180.
6. Alikhan M, Rex D, Khan A, Rahmani E, Cummings O, Ulbright TM. Variable pathologic interpretation of columnar lined esophagus by general pathologists in community practice. Gastrointest Endosc 1999;50:23-26.
7. Borovicka J, Fischer J, Neuweiler J, Netzer P, Gschossmann J, Ehmann T, et al. Autofluorescence endoscopy in surveillance of Barrett's esophagus: a multicenter randomized trial on diagnostic efficacy. Endoscopy 2006;38:867-872.
8. DaCosta RS, Wilson BC, Marcon NE. Fluorescence and spectral imaging. ScientificWorldJournal 2007;7:2046-2071.
9. Curvers WL, Singh R, Song LM, Wolfsen HC, Ragunath K, Wang K, et al. Endoscopic tri-modal imaging for detection of early neoplasia in Barrett's oesophagus: a multi-centre feasibility study using high-resolution endoscopy, autofluorescence imaging and narrow band imaging incorporated in one endoscopy system. Gut 2008;57:167-172.
10. Curvers WL, Herrero LA, Wallace MB, Wong Kee Song LM, Ragunath K, Wolfsen HC, et al. Endoscopic tri-modal imaging is more effective than standard endoscopy in identifying early-stage neoplasia in Barrett's esophagus. Gastroenterology 2010;139:1106-1114.
11. Curvers WL, van Vilsteren FG, Baak LC, Bohmer C, Mallant-Hent RC, Naber AH, et al. Endoscopic trimodal imaging versus standard video endoscopy for detection of early Barrett's neoplasia: a multicenter, randomized, crossover study in general practice. Gastrointest Endosc 2011;73:195-203.
12. Bigio IJ, Mourant JR. Ultraviolet and visible spectroscopies for tissue diagnostics: fluorescence spectroscopy and elastic-scattering spectroscopy. Phys Med Biol 1997;42:803-814.
13. Wagnieres GA, Star WM, Wilson BC. In vivo fluorescence spectroscopy and imaging for oncological applications. Photochem Photobiol 1998;68:603-632.
14. Ramanujam N. Fluorescence spectroscopy of neoplastic and non-neoplastic tissues. Neoplasia 2000;2:89-117.
15. Schomacker KT, Frisoli JK, Compton CC, Flotte TJ, Richter JM, Nishioka NS, et al. Ultraviolet laser-induced fluorescence of colonic tissue: basic biology and diagnostic potential. Lasers Surg Med 1992;12:63-78.
16. Bottiroli G, Croce AC, Locatelli D, Marchesini R, Pignoli E, Tomatis S, et al. Natural fluorescence of normal and neoplastic human colon: a comprehensive "ex vivo" study. Lasers Surg Med 1995;16:48-60.
17. Cothren RM, Richards-Kortum R, Sivak MV, Jr., Fitzmaurice M, Rava RP, et al. Gastrointestinal tissue diagnosis by laser-induced fluorescence spectroscopy at endoscopy. Gastrointest Endosc 1990;36:105-111.
18. Richards-Kortum R, Rava RP, Petras RE, Fitzmaurice M, Sivak M, Feld MS. Spectroscopic diagnosis of colonic dysplasia. Photochem Photobiol 1991;53:777-786.
19. Zangaro RA, Silveira L, Manoharan R, Zonios G, Itzkan I, Dasari RR, et al. Rapid multiexcitation fluorescence spectroscopy system for in vivo tissue diagnosis. Appl Opt 1996;35:5211-5219.
20. DaCosta RS, Andersson H, Wilson BC. Molecular fluorescence excitation-emission matrices relevant to tissue spectroscopy. Photochem Photobiol 2003;78:384-392.
21. Li BH, Xie SS. Autofluorescence excitation-emission matrices for diagnosis of colonic cancer. World J Gastroenterol 2005;11:3931-3934.
22. Wang CY, Chiang HK, Chen CT, Chiang CP, Kuo YS, Chow SN. Diagnosis of oral cancer by light-induced autofluorescence spectroscopy using double excitation wavelengths. Oral Oncol 1999;35:144-150.
23. Chaturvedi P, Majumder SK, Krishna H, Muttagi S, Gupta PK. Fluorescence spectroscopy for

noninvasive early diagnosis of oral mucosal malignant and potentially malignant lesions. J Cancer Res Ther 2010;6:497-502.

24. Gillenwater A, Jacob R, Ganeshappa R, Kemp B, El-Naggar AK, Palmer JL, et al. Noninvasive diagnosis of oral neoplasia based on fluorescence spectroscopy and native tissue autofluorescence. Arch Otolaryngol Head Neck Surg 1998;124:1251-1258.
25. Schwarz RA, Gao W, Stepanek VM, Le TT, Bhattar VS, Williams MD, et al. Prospective evaluation of a portable depth-sensitive optical spectroscopy device to identify oral neoplasia. Biomed Opt Express 2010;2:89-99.
26. Betz CS, Mehlmann M, Rick K, Stepp H, Grevers G, Baumgartner R, et al. Autofluorescence imaging and spectroscopy of normal and malignant mucosa in patients with head and neck cancer. Lasers Surg Med 1999;25:323-334.
27. Ramanujam N, Mitchell MF, Mahadevan A, Warren S, Thomsen S, Silva E, et al. In vivo diagnosis of cervical intraepithelial neoplasia using 337-nm-excited laser-induced fluorescence. Proc Natl Acad Sci U S A 1994;91:10193-10197.
28. Ramanujam N, Mitchell MF, Mahadevan-Jansen A, Thomsen SL, Staerkel G, Malpica A, et al. Cervical precancer detection using a multivariate statistical algorithm based on laser-induced fluorescence spectra at multiple excitation wavelengths. Photochem Photobiol 1996;64:720-735.
29. Tumer K, Ramanujam N, Ghosh J, Richards-Kortum R. Ensembles of radial basis function networks for spectroscopic detection of cervical precancer. IEEE Trans Biomed Eng 1998;45:953-961.
30. Drezek R, Brookner C, Pavlova I, Boiko I, Malpica A, Lotan R, et al. Autofluorescence microscopy of fresh cervical-tissue sections reveals alterations in tissue biochemistry with dysplasia. Photochem Photobiol 2001;73:636-641.
31. Zeng H, Petek M, Zorman MT, McWilliams A, Palcic B, Lam S. Integrated endoscopy system for simultaneous imaging and spectroscopy for early lung cancer detection. Opt Lett 2004;29:587-589.
32. Lam S, Kennedy T, Unger M, Miller YE, Gelmont D, Rusch V, et al. Localization of bronchial intraepithelial neoplastic lesions by fluorescence bronchoscopy. Chest 1998;113:696-702.
33. Hung J, Lam S, Leriche JC, Palcic B. Autofluorescence of normal and malignant bronchial tissue. Lasers Surg Med 1991;11:99-105.
34. Lam S, Macaulay C, Palcic B. Detection and localization of early lung cancer by imaging techniques. Chest 1993;103:12S-14S.
35. Panjehpour M, Overholt BF, Schmidhammer JL, Farris C, Buckley PF, Vo-Dinh T. Spectroscopic diagnosis of esophageal cancer: new classification model, improved measurement system. Gastrointest Endosc 1995;41:577-581.
36. Bourg-Heckly G, Blais J, Padilla JJ, Bourdon O, Etienne J, Guillemin F, et al. Endoscopic ultraviolet-induced autofluorescence spectroscopy of the esophagus: tissue characterization and potential for early cancer diagnosis. Endoscopy 2000;32:756-765.
37. Pfefer TJ, Paithankar DY, Poneros JM, Schomacker KT, Nishioka NS. Temporally and spectrally resolved fluorescence spectroscopy for the detection of high grade dysplasia in Barrett's esophagus. Lasers Surg Med 2003;32:10-16.
38. Panjehpour M, Overholt BF, Vo-Dinh T, Haggitt RC, Edwards DH, Buckley FP. Endoscopic fluorescence detection of high-grade dysplasia in Barrett's esophagus. Gastroenterology 1996;111:93-101.
39. Georgakoudi I, Jacobson BC, Van DJ, Backman V, Wallace MB, Muller MG, et al. Fluorescence, reflectance, and light-scattering spectroscopy for evaluating dysplasia in patients with Barrett's esophagus. Gastroenterology 2001;120:1620-1629.
40. Georgakoudi I, Jacobson BC, Muller MG, Sheets EE, Badizadegan K, Carr-Locke DL, et al. NAD(P)H and collagen as in vivo quantitative fluorescent biomarkers of epithelial precancerous changes. Cancer Res 2002;62:682-687.
41. Kara M, DaCosta RS, Wilson BC, Marcon NE, Bergman J. Autofluorescence-based detection of early neoplasia in patients with Barrett's esophagus. Dig Dis 2004;22:134-141.
42. Vo-Dinh T, Panjehpour M, Overholt BF, Farris C, Buckley FP, Sneed R. In vivo cancer diagnosis of the esophagus using differential normalized fluorescence (DNF) indices. Lasers Surg Med 1995;16:41-47.
43. Panjehpour M, Overholt BF, Vo-Dinh T, Coppola D. The effect of reactive atypia/inflammation on the laser-induced fluorescence diagnosis of non-dysplastic Barrett's esophagus. Lasers Surg Med 2012;44:390-396.
44. Anandasabapathy S. Novel Endoscopic Techniques for the Detection of Barrett's Dysplasia. Gastrointest Cancer Res 2008;2:81-84.
45. Bogaards A, Aalders MC, Jongen AJ, Sterenborg HJ. Double ratio fluorescence imaging for the detection of early superficial cancers. Rev Sci Instrum 2001;72:3956.
46. Dixon MF. Gastrointestinal epithelial neoplasia: Vienna revisited. Gut 2002;51:130-131.

47. Drezek R, Sokolov K, Utzinger U, Boiko I, Malpica A, Follen M, et al. Understanding the contributions of NADH and collagen to cervical tissue fluorescence spectra: modeling, measurements, and implications. J Biomed Opt 2001;6:385-396.
48. Kara MA, DaCosta RS, Streutker CJ, Marcon NE, Bergman JJ, Wilson BC. Characterization of tissue autofluorescence in Barrett's esophagus by confocal fluorescence microscopy. Dis Esophagus 2007;20:141-150.
49. Roblyer D, Kurachi C, Stepanek V, Williams MD, El-Naggar AK, Lee JJ, et al. Objective detection and delineation of oral neoplasia using autofluorescence imaging. Cancer Prev Res (Phila) 2009;2:423-431.
50. de Veld DC, Skurichina M, Witjes MJ, Duin RP, Sterenborg HJ, Roodenburg JL. Clinical study for classification of benign, dysplastic, and malignant oral lesions using autofluorescence spectroscopy. J Biomed Opt 2004;9:940-950.
51. Kara MA, Peters FP, Fockens P, ten Kate FJ, Bergman JJ. Endoscopic video-autofluorescence imaging followed by narrow band imaging for detecting early neoplasia in Barrett's esophagus. Gastrointest Endosc 2006;64:176-185.
52. Harris DM, Werkhaven J. Endogenous porphyrin fluorescence in tumors. Lasers Surg Med 1987;7:467-472.
53. Cilesiz I, Fockens P, Kerindongo R, Faber D, Tytgat G, Ten KF, et al. Comparative optical coherence tomography imaging of human esophagus: how accurate is localization of the muscularis mucosae? Gastrointest Endosc 2002;56:852-857.
54. Cobb MJ, Hwang JH, Upton MP, Chen Y, Oelschlager BK, Wood DE, et al. Imaging of subsquamous Barrett's epithelium with ultrahigh-resolution optical coherence tomography: a histologic correlation study. Gastrointest Endosc 2010;71:223-230.
55. Barwari K, De Bruin DM, Faber DJ, Van Leeuwen TG, de la Rosette JJ, Laguna MP. Differentiation between normal renal tissue and renal tumours using functional optical coherence tomography: a phase I in vivo human study. BJU Int 2012;110:E415-E420.
56. Wessels R, De Bruin DM, Faber DJ, van Boven HH, Vincent AD, Van Leeuwen TG, et al. Optical coherence tomography in vulvar intraepithelial neoplasia. J Biomed Opt 2012;17:116022.
57. Reif R, Wang RK. Label-free imaging of blood vessel morphology with capillary resolution using optical microangiography. Quant Imaging Med Surg 2012;2:207-212.
58. Patil CA, Kalkman J, Faber DJ, Nyman JS, Van Leeuwen TG, Mahadevan-Jansen A. Integrated system for combined Raman spectroscopy-spectral domain optical coherence tomography. J Biomed Opt 2011;16:011007.